Towards new personalized treatment options for patients with genomically unstable tumors

van Gijn, Stephanie Elise

Analysis of replication stress and ATR inhibitor sensitivity in head and neck squamous-cell carcinomas

4

ABSTRACT

Head and neck squamous cell carcinomas (HNSCCs) are characterized by a high degree of genomic instability, which can be caused by increased levels of replication stress. In this study, we aimed to gain insight into the levels of replication stress in HNSCCs and aimed to identify genes upon which HNSCCs might have become dependent for surviving high levels of replication stress.

Using Functional Genomic mRNA (FGmRNA) profiling, we calculated the degree of genomic instability for 354 HNSCC samples and assessed the association of FGmRNA expression levels of individual genes with the degree of genomic instability. Higher FGmRNA expression of the replication checkpoint kinase ATR was associated with a high degree of genomic instability in HNSCCs. Analysis of the phosphorylation status of RPA, a substrate of ATR, in an independent cohort of 187 HNSCCs and 49 controls further confirmed elevated ATR activity in HNSCCs. Inhibition of ATR reduced cell viability in a panel of HNSCC cell lines suggesting a dependency on ATR. Furthermore, we found that ATR inhibition sensitized HNSCC cell lines to cisplatin treatment which suggests a dependency of HNSCC cells on ATR for stabilizing cisplatin-induced stalled replication forks. Finally, we examined replication fork dynamics in HNSCC cell lines and in fresh *ex vivo* HNSCC tumor samples, which revealed variations in replication fork speed between HNSCCs upon ATR inhibition.

Combined, our results provide a rationale for exploiting the elevated levels of replication stress in HNSCCs as a therapeutic strategy.

INTRODUCTION

Head and neck squamous cell carcinoma (HNSCC) is the sixth most common type of cancer worldwide, accounting for 630,000 new cases and 350,0000 cancer deaths each year[1,2]. Approximately 40% of the HNSCC patients are diagnosed with early stage disease, whereas around 50% are diagnosed with locally-advanced disease and ~10% with distant metastases[3]. While early stage disease is associated with cure rates of ~60-90%, the majority of locally-advanced tumors recur or develop into metastatic tumors despite multi-modality treatment[4]. Although the prognosis of recurrent HNSCC patients improved with the use of the immune checkpoint inhibitor nivolumab[4], only ~20% of the patients appear to respond to immune checkpoint inhibitors[5]. Clearly, there is still an unmet need for better treatment options for recurrent HNSCC patients.

HNSCC cancers are characterized by a high degree of genomic instability[6], which refers to the acquisition of genomic alterations such as somatic copy number alterations (SCNAs) and complex genomic rearrangements[7,8]. Several factors can contribute to genomic instability[9]. An important factor underlying genomic instability in HNSCCs is replication stress, which involves the slowing or stalling of replication fork progression[10-12]. Replication stress can be caused by loss of cell cycle checkpoint control or the activation of certain oncogenes[12]. Increased expression of certain proto-oncogenes, including *c-MYC* and *E2F1*, have been shown to aberrantly activate the initiation of DNA replication and thus lead to replication fork stalling[13,14]. Similarly, loss of tumor suppressor genes, including the frequently inactivated *TP53* and *CDKN2A* genes, cause premature S-phase entry, which negatively impacts on DNA replication fidelity[15,16]. Notably, infection with human papillomavirus (HPV), which is the causal oncogenic event in a subgroup of HNSCCs, also leads to replication stress. Specifically, expression of viral HPV oncogenes E6 and E7 cause aberrant initiation of replication origins, leading to nucleotide pool depletion and consequent replication stress[17]. In addition, expression of HPV oncoproteins induces replication stress by interfering with cell cycle checkpoint control, while preventing p53-dependent apoptosis[18].

Clearly, the etiology of HNSCC is complex, since multiple underlying genetic or viral factors have been shown to be involved in the induction of replication stress. A number of replication stress-targeted agents are currently being tested in clinical trials and show clinical activity in HNSCCs, including inhibitors of the replication checkpoint kinases ATR, Chk1 and Wee1[19,20]. However, it is currently unclear how these drugs can be optimally used, and how patients should be selected[21]. Also, it is currently unclear what the extent and inter-tumor heterogeneity of replication stress levels

is in HNSCCs.

Evidently, there is a need for assays that can accurately predict therapy response to such agents, which could improve treatment for HNSCC patients. The aim of this study was to assess the levels of replication stress in HNSCCs, and to unravel which genes or pathways HNSCC cells have become dependent on for their survival.

RESULTS

Identification of genes of which FGmRNA levels are associated with the degree of genomic instability

We hypothesized that genes that show elevated expression in genomically unstable HNSCCs may be part of an adaptation response of HNSCCs to survive lethal levels of genomic instability. To this end, we retrieved 354 HNSCC samples from the GEO omnibus from 9 different data sets (Table 1, Suppl. Table 1) and applied functional genomic mRNA (FGmRNA) profiling. We subsequently calculated a univariate measure (GI-index) that represents the degree of genomic instability per sample (Fig. 1A). A large variation in the degree of genomic instability across HNSCC samples was observed ranging from 0.8 to 1.5, which contrasted to GI-indices of normal mucosa samples, which ranged from 0.8 to 0.86 (Fig. 1B). Subsequently, we performed a transcriptomic-wide association study (TWAS) to assess the association between FGmRNA expression of individual genes and the degree of genomic instability (Fig. 1C). Ranking of genes based on their association with the degree of genomic instability, resulted in a list of genes of which the top 10 genes are presented in Table 2. We analyzed expression of these 10 genes in 279 HNSCC samples from The Cancer Genome Atlas[6], to determine which of these genes is most frequently upregulated on mRNA level and amplified on DNA level in HNSCCs. *ARMC8*, a gene involved in cell migration, proliferation and tissue maintenance[26] was most often altered (32% of TCGA HNSCC samples), which most frequently involved mRNA upregulation and somatic copy number (SCN) amplification (Supplemental Fig. 1). Similarly, the replication stress kinase *ATR* showed genomic alterations in 31% of the samples, again mostly involving mRNA upregulation and SCN amplification (Supplemental Fig. 1). Since FGmRNA levels of *ATR* showed a stronger association with genomic instability (ranked 7th) than ARMC8 (ranked 8th), combined with the notion that *ATR* plays a role in replication stress, we further focused on *ATR*.

Serial identifier	*Platform identifier*	*Number of samples*
GSE9600	*GPL570*	*4*
GSE1722	*GPL96*	*6*
GSE3524	*GPL96*	*16*
GSE2280	*GPL96*	*21*
GSE9844	*GPL570*	*25*
GSE6791	*GPL570*	*41*
GSE30784	*GPL570*	*70*
GSE42743	*GPL570*	*74*
GSE41613	*GPL570*	*97*
	total	*354*

Table 1: List of different data sets from the GEO omnibus that were used to retrieve HNSCC samples.

	Gene symbol	*Chromosomal locus*	*Z-score*
1	*SRGN*	*10q22.1*	*13.84*
2	*COL3A1*	*2q31*	*13.82*
3	*TNFSF10*	*3q26*	*13.29*
4	*RGS1*	*1q31*	*13.22*
5	*RPL8*	*8q24.3*	*12.86*
6	*LUM*	*12q21.3-q22*	*12.40*
7	*ATR*	*3q23*	*12.23*
8	*ARMC8*	*3q22.3*	*12.16*
9	*PLAG1*	*8q12*	*12.15*
10	*NID1*	*1q43*	*12.04*

Table 2: List of the top 10 most elevated genes of which high FGmRNA are associated with a high degree of genomic instability.

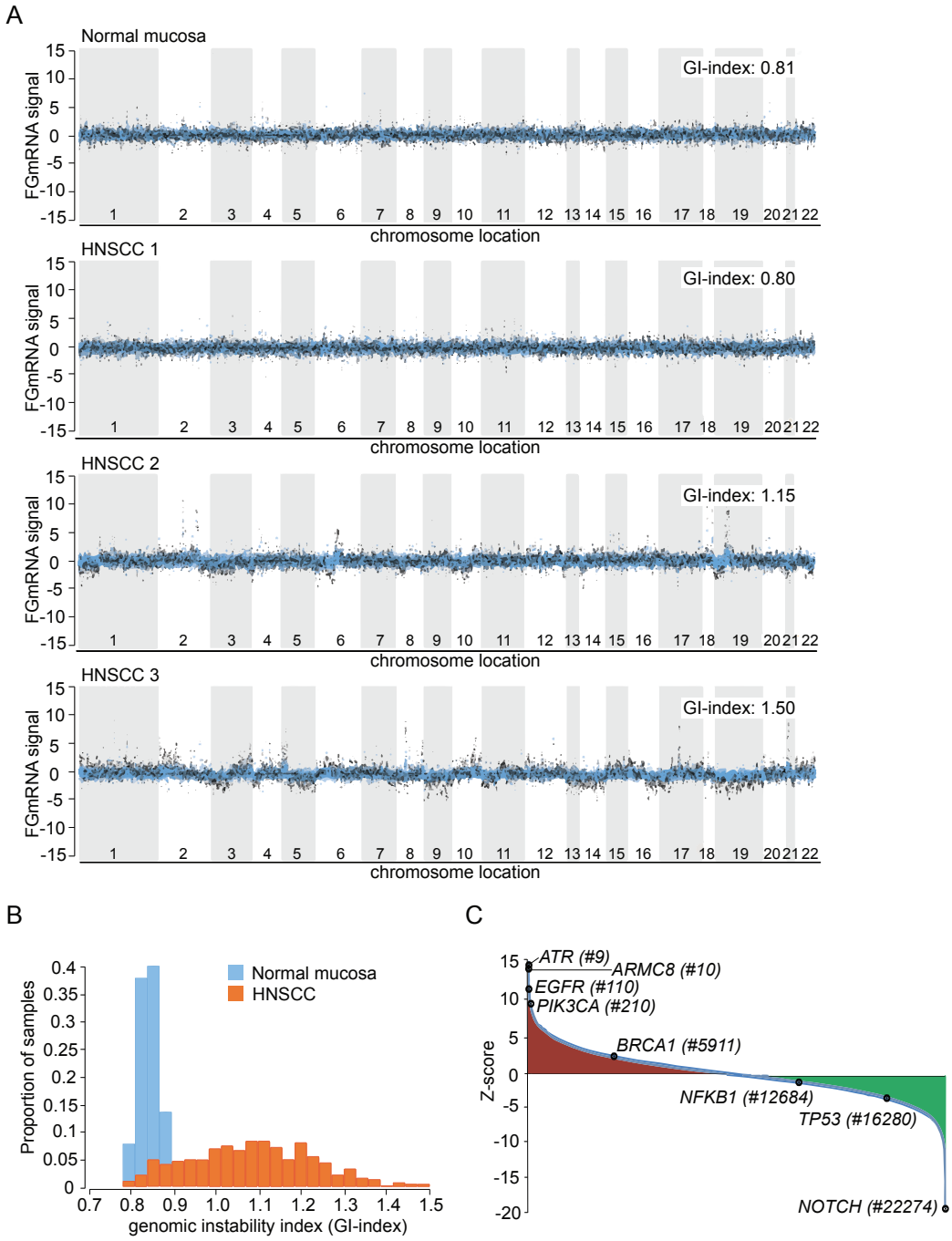

Figure 1: Associations with genomic instability. (A) FGmRNA expression profiles of three HNSCC samples and a normal mucosa sample. Predicted duplications and deletions per region on the chromosome are identified by distinct peaks or valleys, respectively. The genomic instability index (GI-index), a univariate score for the degree of genomic instability, is indicated in each profile. (B) Genomic instability index (GI-index) of normal mucosa and HNSCC samples. (C) Genes assorted to their association between FGmRNA expression levels and the degree of genomic instability (Z-score).

HNSCCs have elevated levels of phospho-RPA

ATR is activated at stalled replication forks, which are marked by increased amounts of single-stranded DNA (ssDNA). SsDNA stretches are rapidly coated by the trimeric RPA protein complex[11,27,28] of which ATR phosphorylates the RPA2 subunit at Ser-33, triggering a feed-forward loop to further activate ATR and its substrate Chk1 at replication forks[29]. As a proxy for ATR activity in HNSCCs and an indirect readout for replication stress, we examined the levels of phospho-RPA2-Ser33 (further referred to as pRPA)[30] in an independent patient cohort containing 187 treatment-naïve HNSCC samples. pRPA staining could be assessed in 171 out of 187 samples (91.4%), with 2.8 assessable cores per case on average. Patient and tumor characteristics of assessable cores are presented in Table 3. As expected, pRPA staining was observed in the nuclei of tumor cells. No cytoplasmic pRPA staining was detected, and pRPA staining was not detected in stromal cells. Examples of pRPA staining reflecting predominantly negative or predominantly positive tissue cores are shown in Fig. 2A. In 85.3% of the tumor samples, some degree of nuclear pRPA staining was detected. Waterfall plot analysis of all the samples did not show segregation into clear subgroups, except for those samples with no pRPA staining (n=25) and samples of which all tumor cell nuclei stained positive for pRPA (n=9) (Fig. 2B). Taken together, the majority of tumor cells in HNSCC samples showed pRPA staining, in contrast to stromal cells or normal tissue (data not shown), suggesting that the ATR-Chk1 signaling pathway is activated in the large majority of HNSCCs.

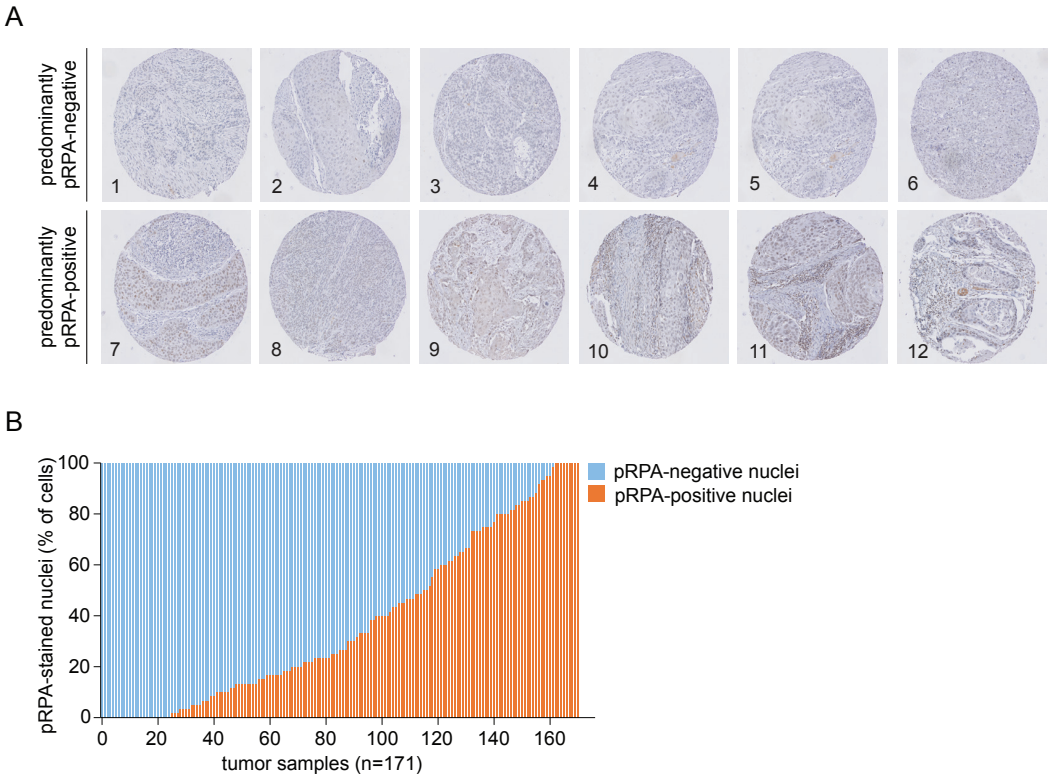

Figure 2: Immunohistochemical staining of pRPA. (A) Representative images of pRPA staining on HNSCC samples. Tissue cores 1-6 show predominantly negative staining (0), cores 7-10 show predominantly positive staining (1+). (B) Waterfall plot showing the distribution of positive and negative pRPA-stained nuclei in a total of 171 HNSCC samples. Percentages of stained nuclei include average pRPA staining of two or three cores.

Table 3: Patient and tumor characteristics of assessable cores stained for pRPA.

	N (%)
No. of patients	171 (100)
Sex	
Male	115 (67)
Female	56 (33)
Age	
Median	60
Range	25-90
Anatomic subsite	
Oral cavity	94 (55)
Oropharynx	29 (17)
Hypopharynx	10 (6)
Larynx	38 (22)
Histological differentiation	
Well differentiated	25 (6)
Moderately differentiated	95(56)
Poorly differentiated	48 (28)
Unknown	3 (2)
T-classification	
1	16 (9)
2	29 (17)
3	38 (22)
4	88 (51)
N-classification	
Negative	48 (28)
Positive	108 (63)
Missing	15 (9)
Stage	
I/II	25 (15)
III/IV	146 (85)

Data were retrieved from a cohort reported previously[24].

ATR inhibition potentiates cisplatin sensitivity in HNSCC cell lines

Since ATR is frequently upregulated or amplified in HNSCCs according to the TCGA HNSCC dataset, we hypothesized that HNSCCs may depend on ATR to survive in conditions of increased replication stress levels. To test whether HNSCCs depend on ATR for their survival, we treated six HNSCC cell lines with the ATR inhibitor VE-821. Cell line characteristics of the six HNSCC cell lines, including primary location, previous treatment, grade and HPV status, are presented in Table 4. Short-term assessment of ATR inhibitor sensitivity showed that all tested HNSCC cell lines were only very moderately sensitive to single agent ATR inhibition, albeit to varying extent (Fig. 3A). In comparison, hardly any cytotoxicity was observed in non-transformed hTERT RPE-1 cells (Fig. 3A). In contrast to short-term assays, long-term clonogenic assays did show sensitivity of HNSCC cell lines to single agent ATR inhibition (Fig. 3B). We next assessed whether ATR inhibition sensitized HNSCC cell lines to cisplatin (Fig. 3B). Strikingly, all HNSCC cell lines, ecxept non-transformed RPE-1 cells, showed robust potentiation of cisplatin sensitivity upon ATR inhibition (Fig. 3C). Combined, these results show that HNSCC cells are moderately sensitive to single-agents ATR inhibition, but display robust cisplatin sensitization upon ATR inhibition.

Table 4: HNSCC cell line characteristics.

Cell line	Primary location	Mutational status	Previous treatment	Grade	HPV status
UT-SCC9	glottic larynx	p53 disruptive mut.	RT	I	neg.
SCC9	tongue	p53 frameshift mut.	no	?	neg.
UT-SCC24a	tongue	p53 frameshift mut.	no	II	neg.
VU-SCC078	floor of the mouth	p53 wt	RT/CT	II	neg.
FaDu	pharynx	p16 mut., p53 missense mut.	?	?	neg.
UT-SCC23	glottic larynx	p53 missense mut.	RT	I	neg.

(wt=wild type, mut.=mutation, ?=unknown, RT=radiotherapy, CT=chemotherapy, neg.=negative)

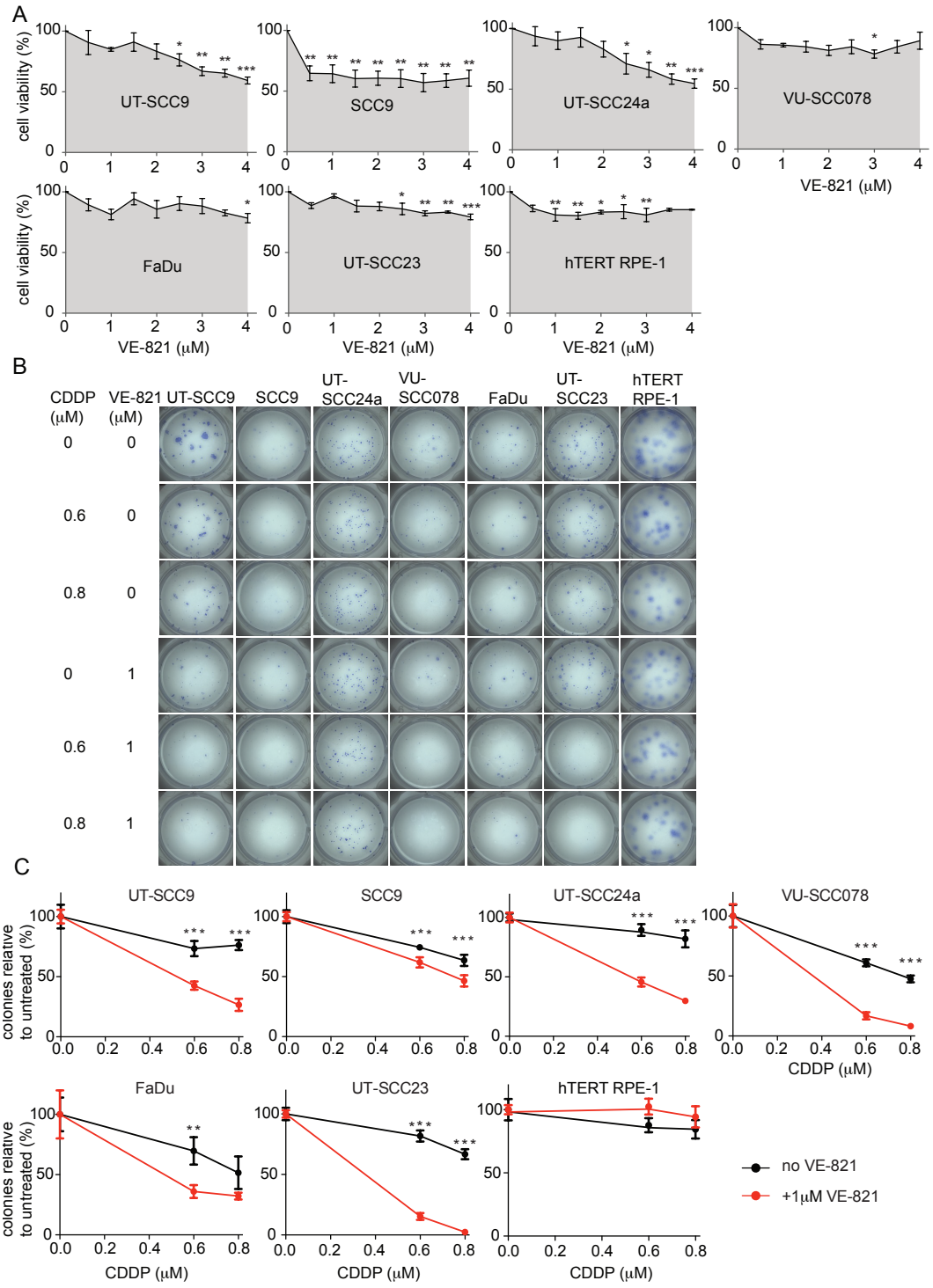

Figure 3: ATR inhibition potentiates cisplatin sensitivity in HNSCC cell lines. (A) Short-term cell viability assays of HNSCC cell lines and a normal retina epithelial cell line (hTERT-RPE-1) treated with varying concentrations of VE-821 for 72 hours. Shown graphs are representative of three independent experiments with three technical replicates each. Means and standard error of the means are depicted.

An ANOVA with Bonferroni multiple comparisons test was performed for each cell line to test for significant differences in cell viability between treated and untreated cells (*= p≤0.05, **= p≤0.01, ***=p≤0.001). (B) Long-term clonogenic assay of HNSSC cell lines and hTERT-RPE-1 treated with 0.6 or 0.8 μM cisplatin for 24 hours after which 1 μM VE-821 was added or cells were left untreated for 11 days. (C) Quantification of B. Shown graphs are representative of two independent experiments with three technical replicates each. Means and standard error of the means are depicted. An unpaired t-test was used to test for significance between single and dual treatment (*= p≤0.05, **= p≤0.01, ***=p≤0.001).

ATR inhibitor sensitivity versus replication dynamics in HNSCC cell lines.

The enhanced sensitivity of HNSCC cell lines to cisplatin when combined with ATR inhibition suggests a role for ATR in stabilizing cisplatin-induced stalled replication forks. To test this notion, we measured incorporation of thymidine analogues IdU and CldU at single DNA fibers, as a direct measurement of replication fork speed (Fig. 4A and Suppl. Fig. 2). We found that median replication speed was very comparable between HNSCC cell lines, except for UT-SCC24a, which displayed faster kinetics (Fig. 4B). Notably, ATR inhibition resulted in decreased replication speed in three out of six cell lines (SCC9, UT-SCC9, UT-SCC23, Fig. 4B). In contrast, other HNSCC cell lines showed no significant change in replication speed upon ATR inhibition (VU-SCC078) or a significantly increased replication speed upon ATR inhibition (FaDu and UT-SCC24a) (Fig. 4B). When comparing replication speed kinetics with the cell viability assays (MTT: Fig. 4C and clonogenic assay: Fig. 4D) upon ATR inhibition in the HNSCC cells lines, we found that cells lines which showed strongest sensitivity to ATR inhibition (SCC9, UT-SCC9) also displayed decreased replication fork speed when ATR was inhibited (Fig. 4C, D). In contrast, UT-SCC23, UT-SCC24a and VU-SCC078 cell lines appeared relatively insensitive to ATR inhibition, which corresponded to the absence of a decreased replication fork speed in two cell lines (UT-SCC24a and VU-SCC078) upon ATR inhibition. UT-SCC23 cells displayed a decrease in replication fork speed, although these cells were relative insensitive to ATR inhibition in the viability assays (Fig. 4C, D). FaDu cells appeared only moderately sensitive to ATR inhibition, however, decreased replication fork speed was not observed upon ATR inhibition in these cells. Combined, replication fork dynamics upon ATR inhibition appeared to be correlated to sensitivity to ATR inhibition in four of the six HNSCC cell lines.

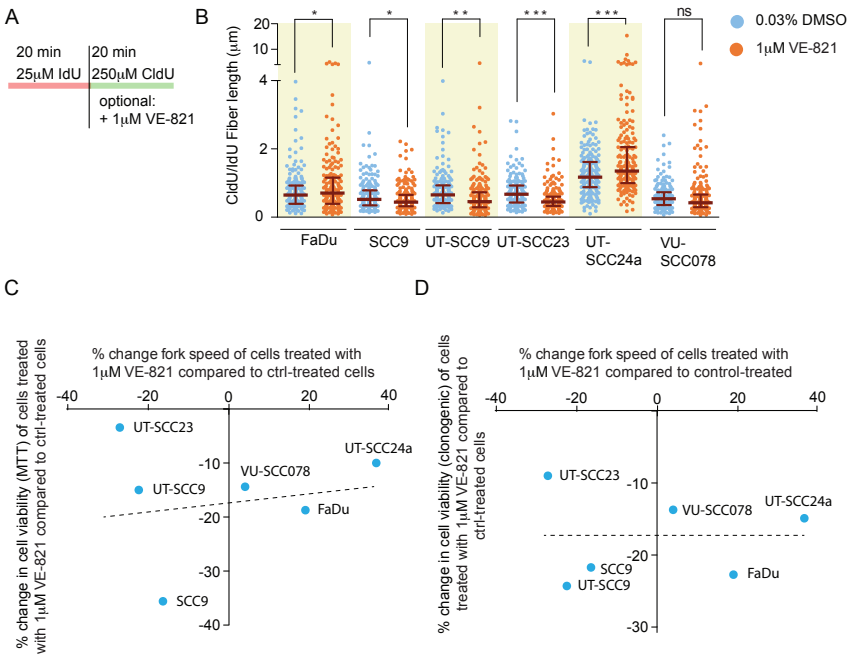

Figure 4: Replication stress levels in HNSCC cell lines. (A) Schematic depiction of addition of synthetic nucleotides with or without VE-821 (B) Ratio CldU/Idu fiber lengths in µm for HNSCC cell lines treated with 1 µM VE-821 or control-treated cells with 0.03% DMSO. 150 to 200 fibers were counted per condition. An unpaired t-test was performed to test for significance (*= p≤0.05, **= p≤0.01, ***=p≤0.001). (C) Correlation of replication fork speed change with change in cell viability (MTT assay) in HNSCC cell lines treated with 1 µM VE-821 relative to control-treated cells. A dotted line indicates the trendline. (D) Correlation of replication fork speed change with change in cell viability (clonogenic assay) in HNSCC cell lines treated with 1 µM VE-821 relative to control-treated cells. A dotted line indicates the trendline.

Analysis of replication dynamics in ex vivo HNSCC samples

Next, we wanted to gain more insight into the degree of replication stress in primary HNSCC tumors. To this end, ten freshly obtained HNSCCs tumor specimens were biopsied *ex vivo* and processed into single cell suspensions (Fig. 5A). Tumor characteristics, including location, previous therapy, local recurrence, T-stage and N-stage are presented in Table 5. Analogous to our analysis of HNSCC cell lines, suspensions of tumor cells were incubated with thymidine analogues CldU and IdU, to label ongoing DNA replication (Fig. 5B). To measure the impact of ATR inhibition, we measured DNA fiber lengths in the absence or presence of ATR inhibitor VE-821 (Fig. 5A and Suppl. Fig. 3). Analysis of replication fork speed showed that fiber length after ATR inhibition significantly decreased in four out of ten tumors, of which three were statistically significant) (Fig. 5C). These data underscore that subsets of HNCSS tumors might depend on ATR activity for DNA replication and may point to ATR inhibitors as a therapeutic strategy in HNSCCs.

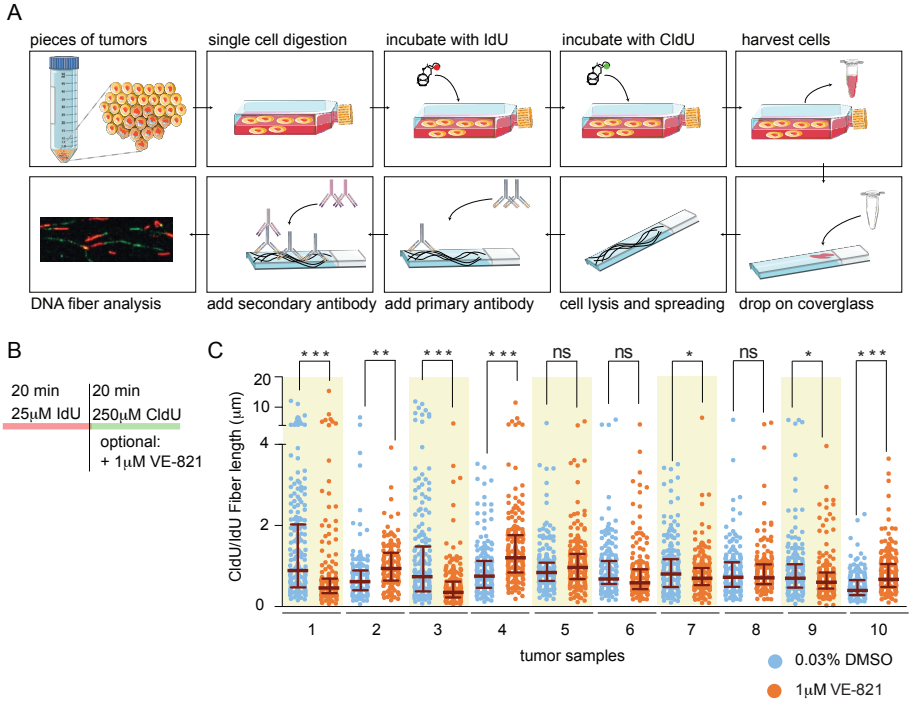

Figure 5: Replication stress in *ex vivo* tumors. (A) Workflow for preparing tumor biopsies for DNA fiber analysis. (B) Schematic depiction of addition of synthetic nucleotides with or without VE-821. (C) Ratio CldU/Idu fiber lengths in µm for HNSCC *ex vivo* tumor biopsies treated with 1 µM VE-821 or control-treated cells with 0.03% DMSO. Between 150 and 200 fibers were counted per condition. An unpaired t-test was performed to test for significance (*= p≤0.05, **= p≤0.01, ***=p≤0.001).

Table 5: *Ex vivo* HNSCC tumor characteristics.

Tumor number	*Location*	*Local recurrence*	*Previous treatment (RT/CHRT)*	*T-stage*	*N-stage*	*Biopsy contains tumor (identified with HE staining)*
1	*larynx*	*yes*	*RT*	*3*	*0*	*?*
2	*oropharynx*	*new primary tumor*	*RT*	*4b*	*?*	*?*
3	*larynx*	*no*	*no*	*4a*	*0*	*?*
4	*larynx*	*no*	*no*	*4a*	*2c*	*yes*
5	*hypopharynx*	*no*	*no*	*4a*	*2b*	*yes*
6	*larynx*	*no*	*no*	*4a*	*0*	*yes*
7	*oropharynx*	*new primary tumor*	*RT*	*2*	*0*	*yes*
8	*larynx*	*no*	*no*	*3*	*1*	*?*
9	*larynx*	*no*	*no*	*4a*	*2b*	*?*
10	*larynx*	*no*	*no*	*4a*	*0*	*?*

(?=unknown, RT=radiotherapy, CHRT=chemoratiotherapy, HE=Hematoxylin-Eosin staining)

DISCUSSION

In this study, we applied FGmRNA profiling to 354 HNSCC samples to assess the degree of genomic instability per HNSCC sample, which was subsequently associated to the FGmRNA expression levels of individual genes. Higher expression of the replication checkpoint kinase ATR was found to be associated with a higher degree of genomic instability. In line with this association, the abundance of phosphorylated RPA, a substrate of ATR, was elevated in a cohort of HNSCCs in comparison to stromal cells or normal tissue where no phosphorylation of RPA was detected. Also, ATR inhibition was found to sensitize all HNSCC cell lines to cisplatin treatment. Furthermore, we found that ATR sensitivity was moderately, positively correlated to replication fork dynamics upon ATR inhibition in the majority of HNSCC cell lines. Finally, we report for the first time on direct measurements of replication fork speed in fresh tumor material at the level of single DNA fibers, which revealed differential sensitivity of replication fork speed to ATR inhibition.

Clonogenic survival analysis in our panel of HNSCC cell lines indicated that ATR inhibition potentiates cisplatin treatment. Several ongoing clinical trials investigate ATR inhibition in combination with DNA damaging agents in a variety of cancers[19]. Currently, patients with recurrent or metastatic HNSCC are treated with cetuximab plus cisplatin/carboplatin and 5-fluorouracil (5-FU) as a first-line treatment. However, patients almost invariably develop resistance to cisplatin/carboplatin treatment. In this context, the observation that ATR inhibition can be used to re-sensitize cisplatin-resistant HNSCCs to cisplatin treatment warrants further evaluation. Encouraging data have been obtained in preclinical studies in triple-negative breast and ovarian cancer cells, which showed that ATR inhibition was able to re-sensitize cisplatin-resistant cells to cisplatin[31,32].

One of the main aims of this study was to gain more insight into the degree of replication stress and the dependency of HNSCCs on ATR. Cancer cells are thought to increasingly depend on cell cycle checkpoint kinases such as ATR and Chk1[13,23,33] in order to deal with enhanced and sustained levels of replication stress. Therapeutic targeting of the ATR-Chk1 signaling pathway is based on the exploitation of replication stress, which arises when stalled replication forks are converted into lethal DNA double strand breaks (DSB) in the absence of a proper replication stress response[11,13,34]. We observed in our study that all HNSCCs cell lines were sensitive- to various degrees- to ATR inhibition which suggests a dependency on ATR, although variations in sensitivity upon ATR inhibition could not be explained with cell line characteristics. As ATR is an essential gene, some sensitivity to ATR inhibition is expected as was also observed in hTERT RPE-1 cells[19].

Measuring the degree of replication stress can be useful to determine the threshold of a tumor from manageable levels of replication stress to lethal levels of replication stress[35]. In this study, we were the first ones to gain insight into the replication fork dynamics of fresh *ex vivo* HNSCC tumors.

We found that ATR inhibition in HNSCCs led in some cases to a decrease, increase or did not change replication fork speed. A decrease in replication fork speed upon ATR inhibition can be explained by replication fork stalling, inability of replication fork stabilization, collapse of replication forks and ultimately cell death[11,13,34]. In some cases, an increase in replication fork speed upon ATR inhibition was observed. Although acceleration of replication fork speed is not as well understood, a recent study showed that an increase of more than 40% in replication fork speed causes DNA damage, which if unrecognized may affect cell viability[36]. Since ATR is also involved in the DNA damage response (DDR) pathway, inhibition of ATR in HNSCCs may affect HNSCCs due to the inability to stabilize stalled replication forks or an inability to recognize replication-induced DNA damage[11,27].

In summary, it will be of interest to see whether the replication stress assay could be implemented as an assay in the clinic predicting response to ATR inhibition in HNSCCs. Since the replication stress essay can be performed on tumors within three days, better predictions on therapy response can be made that could result in higher survival rates of HNSCC patients. Of particular interest will be to determine how well the replication stress assay fits with response to ATR inhibition in HNSCCs. Although, we observed some correlation in HNSCC cell lines, future research should elucidate whether this is also observed in fresh HNSCC biopsies and what other underlying factors *e.g.* previous therapy, TN-stage, secondary genetic aberrations or HPV status can influence replication fork dynamics upon ATR inhibition.

METHODS and MATERIALS

Data acquisition

Publicly available microarray expression profiles were obtained from the Gene Expression Omnibus (GEO). Our analysis was restricted to the Affymetrix Human HG-U133A (GEO accession number GPL96) and Genome U113 Plus 2.0 (GEO accession number GPL570) platform (Affymetrix Inc., Santa Clara, CA, USA). For each individual sample, metadata including patient information and experimental conditions were collected from the Simple Omnibus Format in Text (SOFT) file. HNSCC samples were selected using a two-step approach. Automatic filtering on relevant keywords (as provided in Supplementary Table 1) was performed followed by manual curation. Samples were retained when raw data (CEL files) were available and when samples represented tumor tissue of HNSCC patients. Samples obtained from cell lines, cultured human biopsies and animal samples were excluded. To detect duplicate CEL files, a MD5 hash acting as a unique fingerprint was generated for each CEL file, and duplicate MD5 hash files were removed. Raw data were pre-processed and normalized according to the robust multi-array average algorithm with RMAExpress (version 1.1.0), using the latest CDF file provided by Affymetrix. Quality control of the resulting expression data was performed as previously described[22].

Functional Genomic mRNA Profiling (FGmRNA-profiling)

FGmRNA-profiling was performed as described previously[22]. In short, based on the analysis of 77,840 expression profiles of publicly available samples with principal component analysis (PCA) a limited number of 'Transcriptional Components' (TCs) were shown to capture the major regulators of the mRNA transcriptome. Additionally, a subset of TCs was identified that described non-genetic regulatory factors. These non-genetic TCs were used as covariates to correct microarray expression data (*i.e.* FGmRNA-profile) and revealed the downstream consequences of genomic alterations on gene expression levels.

Assessing the degree of genomic instability per sample

FGmRNA-profiling was used to summarize the total level of chromosomal aberrations in a given HNSCC tumor in a single univariate measure, which was termed the genomic instability index (GI-index)[22,23]. To determine the GI-index per sample, all genes were sorted according to their genomic mapping. Subsequently, a sliding window was applied to the sorted FGmRNA-signals. A sliding window was set to a fixed size of 500K base pairs. Genes that map within this genomic region of

500K base pairs are grouped into a set designated 'A'. The rest of the genes, localized elsewhere on the genome, were grouped into a set 'B'. The functional copy number aberration metric for the given genomic 500K base pair region is the value of the Student's t statistic comparing sets A and B. The sliding window proceeds to the neighboring mapping gene until all genes were at the center of the sliding window once. The sliding window was applied to all chromosomes separately. This method resulted, per individual sample, in a vector, where each element describes the functional copy number aberration degree for a specific genomic region. The sum of the absolute functional copy number aberration metric (*i.e.* T-statistics) resulted in the GI-index.

Association of genes with genomic instability

A genome-wide association analysis was performed between individual genes (*i.e.* functional genomic mRNA expression signal) and the degree of genomic instability (*i.e.* GI-index) in the HNSCC samples. The association was determined by the Pearson product-moment correlation coefficient. To minimize false positive or negative associations due to batch effects (different platforms and experiments), we calculated association statistics within meta-analysis batches. The combination of platform identifier (GPL number, *i.e.* GEO platform accession number), experiment identifier (GSE number, *i.e.* GEO experiment accession number) and tumor type assignment defined a meta-analysis batch. Meta-analysis p-values were calculated according to the Liptak's trend method (Z-transformed p-values, weighted according to the square root of the number of samples in a meta-analysis batch). To assess the degree of multiple testing, we performed this meta-analysis within a multivariate permutation (MVP) test with a false discovery rate of 5% and a confidence level of 80%.

Patient selection and tissue microarray construction

Tissue microarrays (TMAs) were previously established and described, and contained tumor material of HNSCC patients (n=187) and controls (n=49)[24]. Patients were treated at the University Medical Center Groningen between 1997 and 2008 for histologically proven HNSCC and underwent primary tumor resection followed by neck dissection and/or radiotherapy. For TMA construction, the original haematoxylin-eosin stained section from each patient's tumor paraffin block was used for orientation, and representative tumor area were used. Three tissue cores (diameter: 0.6mm) were taken from the tumor and mounted in a recipient block using the Manual Tissue Arrayer I (Beecher Instruments, Sun Prairie, WI).

Immunohistochemistry and grading

Slides were stained using anti-phospho-RPA32-Ser4/Ser8 (abbreviated to pRPA) (1:1,250 dilution; Bethyl, A300-245A) on an automated Benchmark® platform (Ventana Medical Systems, Illkirch, Cedex, France). IgG staining was used as controls and were negative. Antibody staining was evaluated under a light microscope by two independent investigators (SH and SvG) under supervision of a specialized head-and-neck pathologist (BvdV). Tissue cores were excluded for analysis in the absence of tumor cells, improper attachment or insufficient size of the tissue on the cover glass. Discordant cases were re-evaluated in a consensus meeting with all three investigators. From each tumor, three tissue cores were scored to account for intra-tumoral heterogeneity. Samples were scored on percentage of positive tumor cells. Dark brown, coarse staining and light brown staining were classified positive (1+). The absence of pRPA staining in tumor cells was scored negative (0).

Analysis of ex vivo HNSCC material

Pieces of HNSCC tumors (0.5-1cm^2) were received from the operating room at the time of resection. Approval was obtained from Medical Ethical Council of the University Medical Center Groningen (NL 51862.042.15), and informed consent was obtained from all patients. Directly after resection, tumor samples were placed in culture medium consisting of DMEM/F12 (Invitrogen), supplemented with 5% horse serum (Invitrogen), 20ng/mL EGF (Peprotech), 0.5mg/mL hydrocortisone (Sigma), 100ng/mL cholera toxin (Sigma), 1% penicillin/streptomycin (Invitrogen) and 1% Amphotericin B (Gibco) and transferred to the lab. Tumor tissue was washed once in 1x PBS followed by a 30 seconds

incubation in 1x PBS with 25 µg/ml Fungizone. After two PBS wash steps, tumor material was minced into 1-2mm^2 fragments and incubated in culture medium with 1mg/mL collagenase I (Sigma), 1mg/mL collagenase II (Merck Millipore) and 50U/mL DNase (Sigma) on an orbital shaker at 60 rpm at 37ºC and 5% CO_2 for 4-6 hours or until single cell suspensions were obtained. Tumor dissociation was promoted by vigorous pipetting. The single cell suspension was filtered through a 70 µm cell strainer and spun down for 5 minutes at 1000 rpm at 22°C. The cell pellet was resuspended in red blood cell lysis buffer containing 0.16M ammoniumchloride/0.17M Tris pH 7.65 (9:1), and spun down for 5 min. at 1000 rpm at 22°C. The pellet was resuspended in tumor culture media. The obtained cell suspension was used for DNA fiber assays.

DNA fiber analysis

Cells were labeled with 25 µM 5'-Iodo-2-deoxyuridine (IdU, Sigma #I7125) for 20 minutes at 37°C, 5% CO_2, on an orbital shaker (60 rpm). Then, cells were washed twice with warm culture media and were labeled with 250 µM 5-chloro-2deoxyuridine (CldU, Sigma #C6891) for 20 minutes at 37°C, 5% CO_2 , on an orbital shaker (60 rpm) in the presence or absence of 1 µM VE-821 ATR inhibitor. CldU and IdU were dissolved in tumor culture media at stock concentrations of 2.5 mM and 5 mM respectively. IdU was heated to 60°C to promote its solutions in culture media. Replication was stopped by washing twice with ice cold PBS. Cells were counted and diluted to 5*10^5 cells/mL in PBS, and were lysed in lysis buffer (200mM Tris-HCL (pH 7.4), 50mM EDTA and 0.5% SDS), spread on microscopy slides, air-dried and fixed in 3:1 methanol:acetic acid for 10 minutes. Slides were incubated in 2.5M HCL for 1.5 hours, blocked in PBS with 1% BSA and 0.1% Tween for 30 minutes and incubated with primary antibodies rat anti-BrdU (1:1000, Abcam) and mouse anti-BrdU (1:250, BD Biosciences) for 1 hour. Secondary antibodies anti-rat AlexaFluor-488 and anti-mouse AlexaFluor-647 (both 1:500) were incubated for 1.5 hours, prior to analysis on a Zeiss fluorescence microscope (Zeiss LSM 800). Fiber track lengths were measured with ImageJ software.

Cell lines

HNSCC cell lines that were obtained from ATCC were FaDu (pharynx SCC, ATCC HTB-43) and SCC-9 (tongue SCC, ATCC CRL-1629). The UT-SCC-9 (larynx SCC), UT-SCC23 (larynx SCC), UT-SCC24a (tongue SCC) and VU-SCC078 (UPCL-SCC078, floor of mouth SCC) cell lines were a gift and described before[25]. Normal immortalized epithelial retina cells, hTERT-RPE-1 cells were retrieved from ATCC (ATCC CRL-4000). All cell lines were confirmed to be mycoplasma free, and their identity was confirmed using STR profiling. Unless stated otherwise, cell lines were cultured in DMEM low glucose, supplemented with 10% Fetal bovine serum (FBS), 1% glutamin and 1% penicillin/streptomycin. SCC9 cells were cultured in DMEM low glucose:HamF12 (1:1), supplemented with 10% FBS, 1% glutamin, 1% penicillin/streptomycin and 400 ng/mL hydrocortisone. All cells were maintained at 37°C and 5% CO_2.

MTS cell proliferation assay

HNSCC cell lines and hTERT RPE-1 were plated in 96-well plates. FaDu, VU-SCC078 and UT-SCC24a were plated at a density of 1,500 cells per well, UT-SCC23 at 2,000, SCC9 at 4,000 and hTERT RPE-1 and UT-SCC9 at 1,000 cells per well. Cells were allowed to attach for 24 hours and treated with indicated concentrations of VE-821 (AxonMedchem 1893) for 72 hours. CellTiter 96 AQueous One Solution Reagent (Promega G3582) was directly added to the culture media in a 1:10 dilution and incubated for 2 hours at 37°C, 5% CO_2. To measure formazan production, absorbance was recorded at 490nm using a Bio-Rad benchmark III Biorad microtiter spectrophotometer. Proliferation was determined as the relative decrease in signal compared to DMSO-treated cells.

Clonogenic survival assay

HNSCC cell lines and hTERT RPE-1 were plated in 6-well plates. hTERT RPE-1 were plated at a density of 100 cells per well, UT-SCC9 at 150, VU-SCC078, UT-SCC23 and UT-SCC24a at 200, SCC9 at 400 and FaDu at 800 cells per well. Cells were allowed to attach for 24 hours and treated with indicated concentrations of cisplatin (Accord) in the absence or presence of VE-821 (1 µM). Cisplatin

was washed away after 24 hours and cells were thereafter treated with 1 μM VE-821 or were left untreated for eleven days. Subsequently, cells were fixed with methanol and stained with staining buffer containing 50% methanol, Coomassie Brilliant Blue (Biorad #1610406) and 20% acetic acid. Colonies were counted manually, and colonies containing more than approximately 50 cells were included.

REFERENCES

1. Ferlay, J. et al. Cancer incidence and mortality worldwide: Sources, methods and major patterns in GLOBOCAN 2012. Int. J. Cancer 136, E359–E386 (2014).
2. Vigneswaran, N. & Williams, M. D. Epidemiologic Trends in Head and Neck Cancer and Aids in Diagnosis. Oral and Maxillofacial Surgery Clinics of North America 26, 123–141 (2014).
3. Ferlay, J. et al. Cancer incidence and mortality worldwide: Sources, methods and major patterns in GLOBOCAN 2012. Int. J. Cancer 136, E359–E386 (2014).
4. Specenier, P. Nivolumab in squamous cell carcinoma of the head and neck. Expert Rev Anticancer Ther 18, 409–420 (2018).
5. Samra, B., Tam, E., Baseri, B. & Shapira, I. Checkpoint inhibitors in head and neck cancer: current knowledge and perspectives. J. Investig. Med. 66, 1023–1030 (2018).
6. Network, T. C. G. A. Comprehensive genomic characterization of head and neck squamous cell carcinomas. Nature 517, 576–582 (2015).
7. Santaguida, S. et al. Chromosome Mis-segregation Generates Cell-Cycle-Arrested Cells with Complex Karyotypes that Are Eliminated by the Immune System. Dev. Cell 41, 638–651.e5 (2017).
8. Negrini, S., Gorgoulis, V. G. & Halazonetis, T. D. Genomic instability — an evolving hallmark of cancer. Nat. Rev. Mol. Cell Biol. 11, 220–228 (2010).
9. Langie, S. A. S. et al. Causes of genome instability: the effect of low dose chemical exposures in modern society. Carcinogenesis 36 Suppl 1, S61–88 (2015).
10. Aguilera, A. & Gómez-González, B. Genome instability: a mechanistic view of its causes and consequences. Nat. Rev. Genet. 9, 204–217 (2008).
11. Zeman, M. K. & Cimprich, K. A. Causes and consequences of replication stress. Nat. Cell Biol. 16, 2–9 (2014).
12. Jenkins, G., O'Byrne, K. J., Panizza, B. & Richard, D. J. Genome stability pathways in head and neck cancers. Int J Genomics 2013, 464720–19 (2013).
13. Dobbelstein, M. & Sørensen, C. S. Exploiting replicative stress to treat cancer. Nat Rev Drug Discov 14, 405–423 (2015).
14. Bertoli, C., Skotheim, J. M. & de Bruin, R. A. M. Control of cell cycle transcription during G1 and S phases. Nat. Rev. Mol. Cell Biol. 14, 518–528 (2013).
15. Yeo, C. Q. X. et al. p53 Maintains Genomic Stability by Preventing Interference between Transcription and Replication. Cell Rep 15, 132–146 (2016).
16. Zhang, J., Dai, Q., Park, D. & Deng, X. Targeting DNA Replication Stress for Cancer Therapy. Genes (Basel) 7, 51 (2016).
17. Bester, A. C. et al. Nucleotide deficiency promotes genomic instability in early stages of cancer development. Cell 145, 435–446 (2011).
18. Marullo, R. et al. HPV16 E6 and E7 proteins induce a chronic oxidative stress response via NOX2 that causes genomic instability and increased susceptibility to DNA damage in head and neck cancer cells. Carcinogenesis 36, 1397–1406 (2015).
19. Lecona, E. & Fernandez-Capetillo, O. Targeting ATR in cancer. Nature Reviews Cancer 18, 586 (2018).
20. Qiu, Z., Oleinick, N. L. & Zhang, J. ATR/CHK1 inhibitors and cancer therapy. Radiother Oncol 126, 450–464 (2018).
21. Glorieux, M., Dok, R. & Nuyts, S. Novel DNA targeted therapies for head and neck cancers: clinical potential and biomarkers. Oncotarget 8, 81662–81678 (2017).
22. Fehrmann, R. S. N. et al. Gene expression analysis identifies global gene dosage sensitivity in cancer. Nat. Genet. 47, 115–125 (2015).
23. Krajewska, M. et al. ATR inhibition preferentially targets homologous recombination-deficient tumor cells. Oncogene 34, 3474–3481 (2015).
24. Melchers, L. J. et al. Lack of claudin-7 is a strong predictor of regional recurrence in oral and oropharyngeal squamous cell carcinoma. Oral Oncol. 49, 998–1005 (2013).
25. Lin, C. J. et al. Head and neck squamous cell carcinoma cell lines: established models and rationale for selection. Head Neck 29, 163–188 (2007).
26. Liang, X. et al. Silencing of Armadillo Repeat-Containing Protein 8 (ARMc8) Inhibits TGF-β-Induced EMT in Bladder Carcinoma UMUC3 Cells. Oncol. Res. 25, 99–105 (2017).
27. Zhou, B.-B. S. & Bartek, J. Targeting the checkpoint kinases: chemosensitization versus chemoprotection. Nature Reviews Cancer 4, 216–225 (2004).
28. Toledo, L., Neelsen, K. J. & Lukas, J. Replication Catastrophe: When a Checkpoint Fails because of Exhaustion. Mol. Cell 66, 735–749 (2017).
29. Yekezare, M., Gómez-González, B. & Diffley, J. F. X. Controlling DNA replication origins in response to DNA damage - inhibit globally, activate locally. J. Cell. Sci. 126, 1297–1306 (2013).

30. Murphy, A. K. et al. Phosphorylated RPA recruits PALB2 to stalled DNA replication forks to facilitate fork recovery. J. Cell Biol. jcb.201404111 (2014). doi:10.1083/jcb.201404111
31. Mohni, K. N. et al. A Synthetic Lethal Screen Identifies DNA Repair Pathways that Sensitize Cancer Cells to Combined ATR Inhibition and Cisplatin Treatments. PLoS ONE 10, e0125482 (2015).
32. Sima, N. et al. Small Molecules Identified from a Quantitative Drug Combinational Screen Resensitize Cisplatin's Response in Drug-Resistant Ovarian Cancer Cells. Transl Oncol 11, 1053–1064 (2018).
33. Cottini, F. et al. Synthetic Lethal Approaches Exploiting DNA Damage in Aggressive Myeloma. Cancer Discov 5, 972–987 (2015).
34. Allen, C., Ashley, A. K., Hromas, R. & Nickoloff, J. A. More forks on the road to replication stress recovery. J Mol Cell Biol 3, 4–12 (2011).
35. Andor, N., Maley, C. C. & Ji, H. P. Genomic Instability in Cancer: Teetering on the Limit of Tolerance. Cancer Research 77, 2179–2185 (2017).
36. Maya-Mendoza, A. et al. High speed of fork progression induces DNA replication stress and genomic instability. Nature 559, 279–284 (2018).

HNC	*Oral*	*Tonsillar*	*Gingiva*
Larynx	*Head*	*Mouth*	*Buccal*
Pharynx	*Neck*	*Nose*	*Palate*
Oropharynx	*H&N*	*Nasal*	*Gingival*
Laryngeal	*Nasopharynx*	*Sinus*	*Lip*
Pharyngeal	*Nasopharyngeal*	*Para nasal*	*Epiglottis*
Oropharyngeal	*Tonsil*	*Tongue*	*Cheek*
Glottic	*Supraglottic*	*Glottis*	*Palatal*
Supraglottic	*Subglottic*	*Trachea*	*Epiglottis*
Hypo pharynx	*Hypo pharyngeal*	*Cricoid*	*Vocal*

Supplemental Table 1: Keywords that were used to filter for publically available microarray expression profiles from the Gene Expression Omnibus.

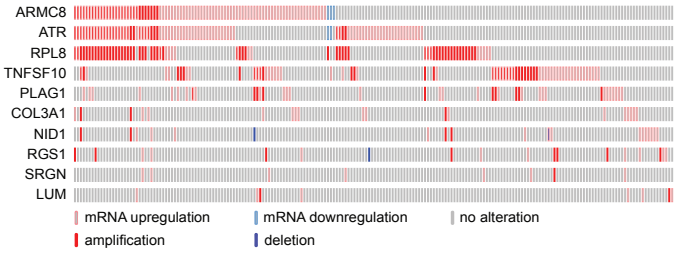

Supplemental Figure 1: Up- and downregulation of mRNA and SCNA (amplifications and deletions) of the ten candidate genes in 279 HNSCC samples from The Cancer Genome Atlas[6].

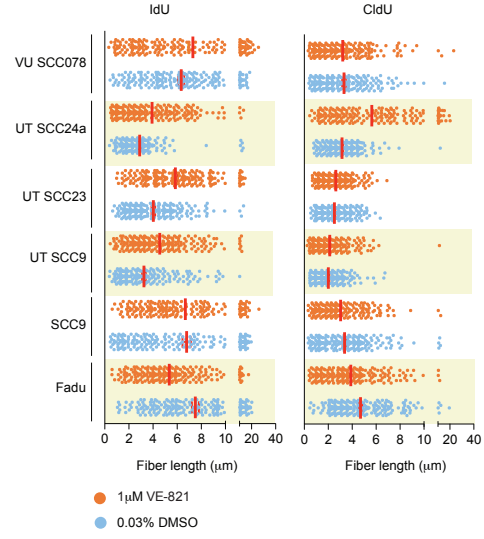

Supplemental Figure 2: CldU and Idu fiber lengths in μm for HNSCC cell lines. Cells were treated with 1 μM VE-821 or control-treated cells with 0.03% DMSO. Between 150 to 200 fibers were counted per condition.

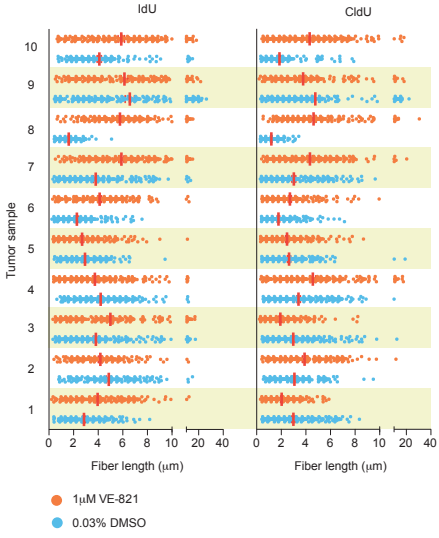

Supplemental Figure 3: CldU and Idu fiber lengths in μm for ten *ex vivo* tumor biopsies. Cells were treated with 1 μM VE-821 or control-treated cells with 0.03% DMSO. Between 150 to 200 fibers were counted per condition.